IEEE Access
Multidisciplinary ⋮ Rapid Review ⋮ Open Access Journal

Received April 24, 2020, accepted May 5, 2020, date of publication May 11, 2020, date of current version May 21, 2020.

Digital Object Identifier 10.1109/ACCESS.2020.2993612

Dual-Point Technique for Multi-Trap RTN Signal Extraction

XUEPENG ZHAN[1,3], YIFANG XI[1], QIANWEN WANG[1], WEIQIANG ZHANG[1], ZHIGANG JI[2], (Member, IEEE), AND JIEZHI CHEN[1], (Senior Member, IEEE)

[1]School of Information Science and Engineering (ISE), Shandong University, Qingdao 266237, China
[2]School of Microelectronics, Shanghai Jiao Tong University, Shanghai 200240, China
[3]State Key Laboratory of High-End Server and Storage Technology, Jinan 250101, China

Corresponding author: Jiezhi Chen (chen.jiezhi@sdu.edu.cn)

This work was supported in part by the China Key Research and Development Program under Grant 2016YFA0201800, in part by the National Natural Science Foundation of China under Grant 91964105 and Grant 61874068, in part by the Joint fund for Intelligent Computing of Shandong Natural Science Foundation under Grant ZR2019LZH009, and in part by the Fundamental Research Funds of Shandong University.

ABSTRACT Random telegraph noise (RTN), as one dominant variation source in the ultra-scaled devices, has been attracting much more attention, and its analysis is of great importance to understand the fundamental physical mechanisms. In this work, with the advanced dual-point method, we successfully separate the impacts of each trap in multi-traps correlated RTN, especially for complex anomalous RTN signals. A four-level transfer curve and VG-dependent RTN magnitude are extracted in a two-trap transistor from the sub-threshold region to the linear region. Furthermore, current degradations contributed from each trap of three- and four-level RTN signals are identified and distinguished. The proposed method can be utilized to evaluate multiple traps RTN and explore the underlying physics.

INDEX TERMS Noise measurement, transistors, high-K gate dielectrics.

I. INTRODUCTION

Random Telegraph Noise (RTN) has attracted increasing attentions with the scaling roadmap of device dimension. In the ultra-scaled devices, random dopant fluctuation (RDF) and electrical traps in the gate dielectrics cause significant time-zero and time-dependent variation issues [1]–[3]. RTN induced variability is observed as the randomly drain current fluctuation under the constant gate and drain voltage, of which the parameters are characterized within a certain time, i.e., a measurement window [4], [5]. The RTN magnitudes including current fluctuation (i.e., ΔID) and threshold voltage fluctuation (i.e., ΔVth), have been recognized as dominant degradation factors affecting the performances of devices and circuits [6]–[8]. Moreover, understanding the voltage dependence of RTN magnitudes can provide valuable information in revealing the underlying physical mechanism and predicting time-dependent variability in circuit simulation [9], [10]. To extend the limited information within the measurement window, Franco *et. al.* swept an entire transfer curve immediately after a standard RTN method with the test sequence shown in Fig.1 (a). It is normally required a rigorous selection of devices with a single dominant trap that exhibits a longer timing constant and giant current fluctuation [3]. When it comes to a fast-switching RTN trap, an oscilloscope-based system is adopted for fast-measurement of the VG dependent RTN magnitudes, which is equipped with a dedicated configuration for reducing the background noise disturbance and increasing measurement accuracy [11]. For obtaining an accurate prediction of RTN-induced degradation, we reported a straightforward dual-point method for characterizing a trapped carrier in both n- and p- FETs [12].

However, these works are normally focused on the device with a single active RTN trap, whose current variation is caused by the transitions of a charge between the empty and occupied state. For a multilevel RTN signal, it is too complicated to analyze and investigate the variation issue, considering the multiple RTN traps and their possible coupling effects. Chang *et. al.* reported a four-level RTN characterization in a gate-all-around (GAA) nanowire transistor, in which the depths of the two discrete traps in the gate oxide are identified separately by extracting the relative trapping/de-trapping frequency [13]. Li *et. al.* measured two traps RTN

The associate editor coordinating the review of this manuscript and approving it for publication was Jenny Mahoney.

with different bias conditions and low temperatures [14]. Gong *et. al.* extracted the trap locations and energy levels by analyzing timing constants from the three-level RTN signals [15], [16]. Moreover, Wang *et. al.* explained the complex RTN phenomenon by considering metastable states and trap coupling effect [17], [18]. For better understanding the evaluation of multi-traps degrading behaviors, it is challenging to identify and differentiate each trap under different bias conditions.

In this work, a four-level and full-VG-range transfer curve is obtained from a planar device with two active RTN traps, corresponding to four different capture and emission states. With the advanced dual-point technique, the RTN magnitudes of each individual trap are extracted from the sub-threshold region to the linear region. Moreover, the degradation effect contributed by each trap is identified and extracted from an anomalous temporal current signal with two-, three- and four-level fluctuations, respectively.

II. MATERIALS AND METHOD

The device under test is a high-K/metal-Gate (HK/MG) planar transistor with a channel length/width of 70nm/90nm and an equivalent oxide thickness of 1.65 nm. The test sequence of the proposed dual-point technique is shown in Fig. 1(b). The short-time standard RTN test is performed firstly with a constant gate voltage (VG_RTN), which could provide the stochastic and different trapping states for the traps. The drain current is measured at a high gate voltage (VGH, illustrated by a blue circle), following by a measurement at a low gate voltage (VGL, illustrated by an orange circle). The above procedure can be repeated by sweeping from the sub-threshold region to the linear region (the orange arrow). With the combination of the obvious current fluctuation at VGH and that at varying VGLs, a two-level transfer curve, corresponding to a single trap either trapping or de-trapping, can be plotted. Moreover, the dual-point technique shows good accuracy at the scale of several nano-ampere shown in Fig. 1(c). The transfer curve agrees well with the result measured by sweeping voltage in a device without RTN traps. In the current (at VGH) versus current (at VGL) plot, the centroid identification of the discrete data extracted by K-means clustering algorithm in the previous study [12], which represents the currents measured with a single trap in both charged and empty state. However, some errors might occur for a complex RTN signal in the clustering process, in which it is trying to separate the scattered points with equal variance and minimized distance. For instance, the experimental data are clustered into three groups, which is obviously against the results guided by the dash circle shown in Fig. 1(d). In this work, to analyze multi-traps contributed RTN, we replace the clustering algorithm by the density-based spatial clustering of applications with noise (DBSCAN), which focuses on the sample density rather than the distance-based algorithm (K-means) [19]. DBSCAN can automate the centroid identification at a fast speed with the advantages of suppressing noise point and clustering arbitrary spatial shapes, which

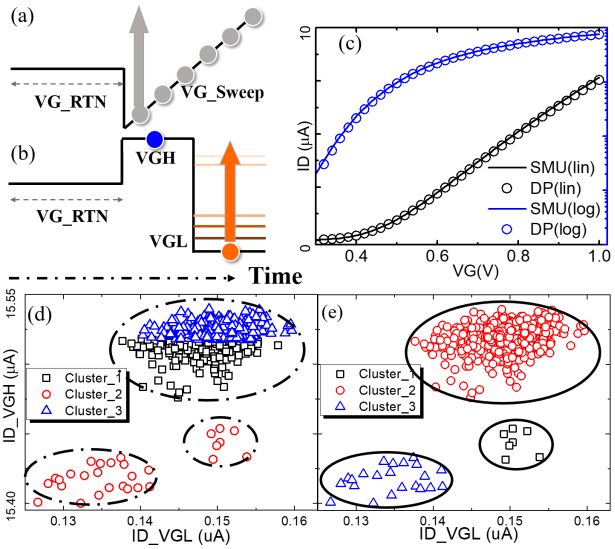

FIGURE 1. Experimental date from dual-point (DP) method: (a&b) Test sequences of sweep voltage and DP method; (c) Transfer curves measured from a device without traps by SMU and DP method, respectively; Measured discrete points clustered by (d) K-means and (e) DBSCAN algorithm, respectively.

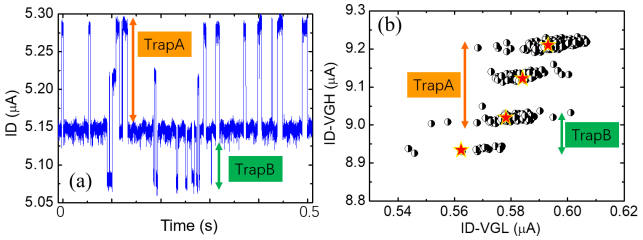

FIGURE 2. RTN signal (a) and measured discrete points (b) from a device with two active RTN traps, which are named as TrapA and TrapB, respectively.

occurs frequently in multi-traps devices considering the traps coupling effect and complex transitions between various current levels. In Fig. 1(e), the measured currents can be well clustered into three groups as expected.

One example is shown in Fig. 2(a). By performing standard RTN measurement under constant (drain and gate) bias condition, the clear four levels can be observed suggesting that there are two discrete RTN traps involved. We marked the one with larger fluctuation as TrapA and the small fluctuation as TrapB, respectively. The highest level (L1) and the lowest level (L4) stand for the situations when the two traps are both empty and occupied, respectively. The second-high level (L2) and third high level (L3) imply that only TrapB or TrapA is occupied, respectively. We applied the advanced dual-point method on this device with one measurement result in Fig. 2(b). Wherein, VGH (0.80 V) is set the same as the aforementioned RTN test and VGL is 0.50V. Vertically, four discrete clusters can be clearly observed corresponding to the four levels in RTN test. Moreover, there is a shift in the parallel direction, suggesting that our measurement also captured the impact of traps on the low voltage level. Due to

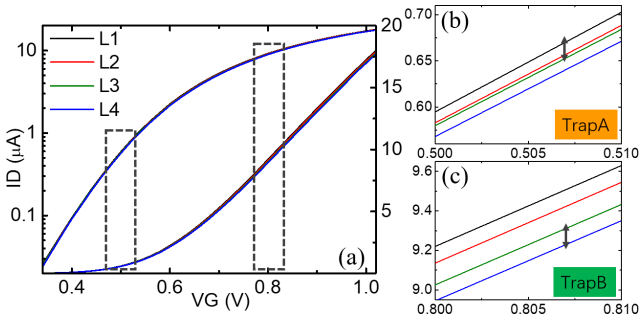

FIGURE 3. (a): A four-level transfer curve of a device with two active RTN traps, whose current fluctuation is caused by TrapA and TrapB, respectively. (b&c) Local zoomed transfer curves in the (b) sub-threshold region and (c) linear region, respectively.

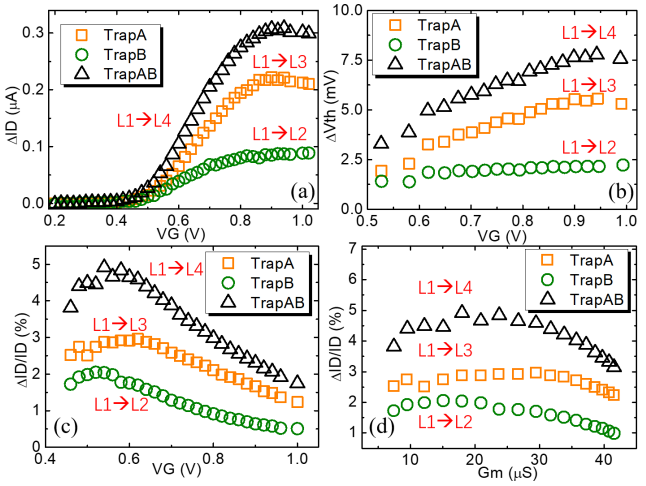

FIGURE 4. The relationship between RTN magnitude and gate voltage in a device with two active traps: (a) ΔID and (b) ΔVth, respectively. The drain current fluctuations versus (c) VG and (d) g_m, respectively.

the measurement accuracy of the testing equipment, there is a wide-spreading for each cluster. We extracted their centroids (illustrated as stars) of the four discrete clusters representing the measured currents at two different voltages (VGH and VGL) with four different states (i.e., L1(00), L2(01), L3(10), and L4(11)), respectively, where 0 being empty and 1 being captured state of a charge. For example, the centroids of the right-top cluster correspond to the (00) state measured at VGH and VGL, respectively.

By fixing VGH and sweeping VGL from the sub-threshold to the linear region, the entire transfer curve can be obtained, as shown in Fig. 3(a). The enlarged two regions at linear and sub-threshold regions are shown in Fig. 3(b&c). The impact of IV curves with two active traps can be observed. With this method, it is easy to confirm the RTN magnitude caused by each individual trap. Under a certain gate voltage, TrapA leads to a larger current fluctuation (from L1 to L3) while TrapB results in a smaller one (from L3 to L4), as arrays shown in Fig. 3(b&c), respectively. Furthermore, the current fluctuation obtained in the advanced dual-point technique (Fig. 3(a)) matches well with the temporal RTN signals in Fig. 2(a). What is worth noting is that the dual-point measurement has successfully identified the difference of 1.5 mV in the sub-threshold region (Fig. 3(b)), which is impossible by standard RTN test. Therefore, this method can simply broaden the measurement window for voltage sweeping down to the sub-threshold region.

III. RESULTS AND DISCUSSION

Based on the obtained four-level transfer curve from the sub-threshold to the linear region, the impacts of individual RTN traps on device performance could be distinguished and studied independently. In the two-RTN-traps device, the TrapA induced current fluctuation (ΔID) is extracted from the transition between L1 (00) and L3 (10), illustrated as the orange square in Fig. 4(a). Similarly, from the transition between L1 (00) and L2 (01), the TrapB induced ΔID under different bias is illustrated as the green circle. The black triangle line corresponds to the relationship between the gate voltage and total ΔID, which is indicating the transition of two traps in empty (L1, (00)) and occupied (L4, (11)) state. Moreover, the total ΔID increases as the gate voltage increases and reduces slightly towards the linear region, whose trend is dominated by the contribution of TrapA and roughly equal with the sum of the contribution of the two individual traps. Similarly, in Fig. 4(b), threshold variations (ΔVth) of each individual trap are compared at different gate voltages. It is observed that TrapB caused ΔVth (L1(00) to L2(01)) is much smaller than that of TrapA (L1(00) to L3(10)). According to the reported 3D atomic simulation [20], [21], these results indicate that TrapA possibly locates nearer to the channel interface. Thus, as the inversion carriers distribute more closer to the channel interface at higher VG, the impacts of TrapA turn to be much more serious. As shown in Fig. 4(c), though the drain current fluctuation ratio weakly depends on VG in the subthreshold region, it shows an obvious decreasing trend in the channel carrier inversion region at higher VG. Generally, the drain current fluctuations can be explained by the carrier number fluctuation model and the mobility fluctuation model [22], [23]. On the one side, the inversion carrier density (N_{inv}) is proportional to (VG-Vth) via $N_{inv} = C_{ox}$ (VG-Vth)/$L_g W_g$, where Vth is the threshold voltage, C_{ox} is the gate-channel capacity, and L_g/W_g is the gate length/width. The roughly linear relationship between the current fluctuations and VG indicates that the number fluctuation contribution is dominant in the inversion region. On the other hand, as shown in Fig. 4(d), the drain current fluctuations weakly depend on the transconductance (g_m), indicating that the drain current fluctuations cannot be explained by the mobility fluctuations. Therefore, the current fluctuations of both traps are mainly contributed by the carrier number fluctuation model. Furthermore, the threshold voltages can be extracted from the discrete transfer curves, which are (L1) 0.5733, (L2) 0.5750, (L3) 0.5761, and (L4) 0.5776 V, respectively. Similarly, the extracted sub-threshold swing (S.S) val-

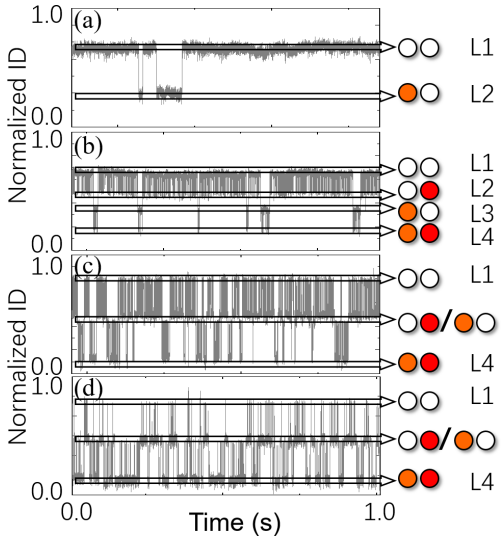

FIGURE 5. RTN signals of a two-trap device with various gate voltages of (a) 0.50 V, (b) 0.60 V, (c) 0.70 V and (d) 0.80 V, respectively.

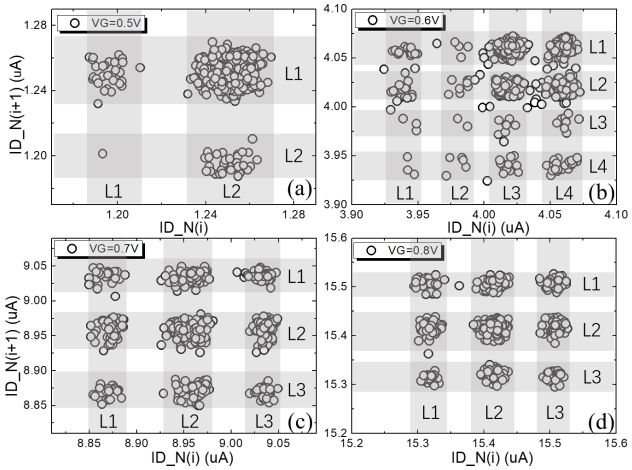

FIGURE 6. Measured discrete points in time-lag plot with different VGL of (a) 0.50 V, (b) 0.60 V, (c) 0.70 V and (d) 0.80 V, respectively.

ues are (L1) 120.76, (L2) 120.37, (L3) 121.22, and (L4) 117.69 mv/decade, respectively.

In another device with an anomalous RTN signal, the temporal current signals are also well investigated with two-, three- and four-level fluctuations, respectively. In Fig. 5, it shows RTN signals with different gate voltages of (a) 0.50 V, (b) 0.60 V, (c) 0.70 V and (d) 0.80 V, respectively. Similarly, the two traps are named as TrapC (larger current fluctuation, orange circle) and TrapD (smaller current fluctuation, red circle), respectively. As illustrated, solid or empty circle means the RTN trap is either in the captured or emitted state.

The two discrete levels correspond to the random emitting or capturing a charge by one trap while the other remains a constant state. When comes to Fig. 5(b), four current levels (i.e., L1, L2, L3, and L4) are clearly observed coming from the different trapping/de-trapping states (i.e., (00), (01), (10), and (11)) of TrapC and TrapD, respectively. As the

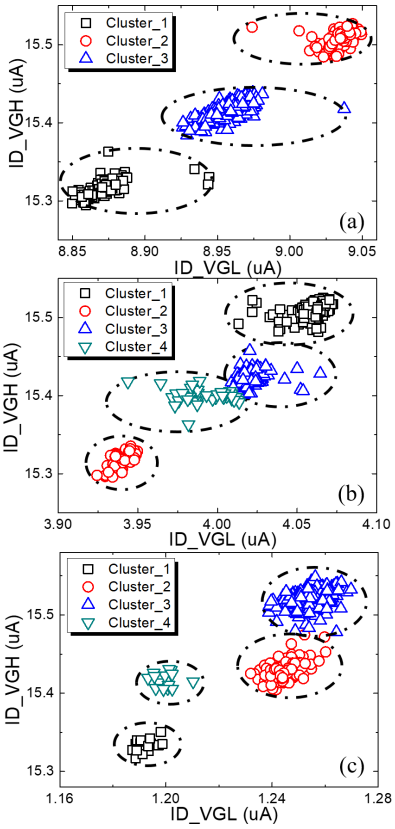

FIGURE 7. Measured discrete points in DP method with constant VGH of 0.80 V and different VGL of (a) 0.70 V, (b) 0.60 V, and (c) 0.50V, respectively.

gate voltage increases, there are only three current levels in Fig. 5(c&d). It is easy to understand that the highest (L1) and lowest (L4) levels correspond to the (00) and (11) states, respectively. Moreover, the medium level is roughly equal with the average of L1 and L4, which might be assigned to the formation of a new coupled state. Nevertheless, it is still not clear whether the medium one comes from the traps coupling effect or the level overlapping between L2 and L3.

Furthermore, the time lag scheme is adopted to facilitate the analysis of the measured signals. Fig. 6 shows the temporal currents in time lag plots, whose x- and y-axis represent the current sampled at a specific time and the next time [24], [25], respectively. From the discrete clusters guided by grey shadow, there are only two trapping/ de-trapping states of one RTN trap in Fig. 6(a), indicating only one trap is detectable while the other is not under the gate voltage of 0.50 V. From the numerous clusters in Fig. 6(b), four different states of two RTN traps are observed with the gate voltage of 0.60 V, matching well with the clear four-level result in Fig 5(b). According to the nine clusters in Fig. 6(c&d), there are only three different states for two individual traps. It is valid that the highest and lowest currents are ascribed to TrapC and TrapD both in the empty (00) and captured (11) states. Whereas the origination of the medium is still unclear for analyzing the trapping/de-trapping state of each trap.

This phenomenon can be well revealed by using the advanced dual-point method. In Fig. 7, the centroid

identifications are extracted under the VGH of 0.80 V and different VGL voltages of (a) 0.70, (b) 0.60, and (c) 0.50 V, respectively. From the current at VGH versus current at VGL plot in Fig. 7(a), the three discrete clusters (guided as dash circles) indicate that only three states are extracted for the gate voltages of 0.80 V and 0.70 V, matching well with the results in Fig. 5(c&d) and Fig. 6(c&d). Benefitted from the clear four current levels at the gate voltage of 0.60 V, four discrete clusters can be seen in Fig. 7(b), indicating the different capture or emission states at the gate voltage of 0.80 V. Although there are only two states at the gate voltage of 0.50 V, four discrete clusters corresponding to different states could be also been in Fig. 7(c). Thus the medium level is distinguished and differentiated, which is more likely to be caused by the overlapping rather than the coupling effect. Noted that the trap coupling effect can be confirmed by exploring the RTN timing constants [26], which is beyond this study and needs further study in detail.

IV. CONCLUSION

With the advanced dual-point technique, a discrete four-level transfer curve from the sub-threshold to the linear region is obtained in a high-κ planar transistor, which corresponds to the four different states of two active RTN traps. The RTN magnitude contributed by each individual trap is extracted in a full-VG-range from sub-threshold to linear region. Moreover, a complex and anomalous RTN signal with two-, three, and four levels is well distinguished and differentiated in this method, which shows the potential ability to explore the RTN trap behaviors and variation issues in a multi-traps device.

REFERENCES

[1] M.-L. Fan, S.-Y. Yang, V. P.-H. Hu, Y.-N. Chen, P. Su, and C.-T. Chuang, "Single-trap-induced random telegraph noise for FinFET, Si/Ge nanowire FET, tunnel FET, SRAM and logic circuits," *Microelectron. Rel.*, vol. 54, no. 4, pp. 698–711, Apr. 2014, doi: 10.1016/j.microrel.2013.12.026.

[2] C. M. Chang, Steve S. Chung, Y. S. Hsieh, L. W. Cheng, C. T. Tsai, G. H. Ma, S. C. Chien, and S. W. Sun, "The observation of trapping and detrapping effects in high-k gate dielectric MOSFETs by a new gate current random telegraph noise (IG-RTN) approach," in *IEDM Tech. Dig.*, no. 2, Dec. 2008, pp. 8–11, doi: 10.1109/IEDM.2008.4796815.

[3] J. Franco, B. Kaczer, M. Toledano-Luque, P. J. Roussel, J. Mitard, L.-A. Ragnarsson, L. Witters, T. Chiarella, M. Togo, N. Horiguchi, G. Groeseneken, M. F. Bukhori, T. Grasser, and A. Asenov, "Impact of single charged gate oxide defects on the performance and scaling of nanoscaled FETs," in *Proc. IEEE Int. Rel. Phys. Symp. (IRPS)*, Apr. 2012, pp. 1–6, doi: 10.1109/IRPS.2012.6241841.

[4] C. Y. Chen, Q. Ran, H.-J. Cho, A. Kerber, Y. Liu, M.-R. Lin, and R. W. Dutton, "Correlation of I_d- and I_g-random telegraph noise to positive bias temperature instability in scaled high-*k*/metal gate n-type MOSFETs," in *Proc. Int. Rel. Phys. Symp.*, Apr. 2011, pp. 190–195, doi: 10.1109/IRPS.2011.5784475.

[5] P. Saraza-Canflanca, J. Martin-Martinez, R. Castro-Lopez, E. Roca, R. Rodriguez, M. Nafria, and F. V. Fernandez, "A detailed study of the gate/drain voltage dependence of RTN in bulk pMOS transistors," *Microelectron. Eng.*, vol. 215, Jul. 2019, Art. no. 111004, doi: 10.1016/j.mee.2019.111004.

[6] C. Liu, K. T. Lee, H. Lee, Y. Kim, S. Pae, and J. Park, "New observations on the random telegraph noise induced Vth variation in nano-scale MOSFETs," in *Proc. IEEE Int. Rel. Phys. Symp.*, Jun. 2014, pp. 4–8.

[7] K. P. Cheung and J. P. Campbell, "On the magnitude of random telegraph noise in ultra-scaled MOSFETs," in *Proc. IEEE Int. Conf. IC Design Technol.*, May 2011, pp. 9–12, doi: 10.1109/ICICDT.2011.5783191.

[8] C. Chen, Q. Huang, J. Zhu, Y. Zhao, L. Guo, and R. Huang, "New understanding of random telegraph noise amplitude in tunnel FETs," *IEEE Trans. Electron Devices*, vol. 64, no. 8, pp. 3324–3330, Aug. 2017, doi: 10.1109/TED.2017.2712714.

[9] B. Kaczer, J. Franco, M. Toledano-Luque, P. J. Roussel, M. F. Bukhori, A. Asenov, B. Schwarz, M. Bina, T. Grasser, and G. Groeseneken, "The relevance of deeply-scaled FET threshold voltage shifts for operation lifetimes," in *Proc. IEEE Int. Rel. Phys. Symp. (IRPS)*, Apr. 2012, pp. 3–8, doi: 10.1109/IRPS.2012.6241839.

[10] I. Zadorozhnyi, J. Li, S. Pud, H. Hlukhova, V. Handziuk, Y. Kutovyi, M. Petrychuk, and S. Vitusevich, "Effect of gamma irradiation on dynamics of charge exchange processes between single trap and nanowire channel," *Small*, vol. 14, no. 2, Jan. 2018, Art. no. 1702516, doi: 10.1002/smll.201702516.

[11] A. Manut, R. Gao, J. F. Zhang, Z. Ji, M. Mehedi, W. D. Zhang, D. Vigar, A. Asenov, and B. Kaczer, "Trigger-when-charged: A technique for directly measuring RTN and BTI-induced threshold voltage fluctuation under use- V_{dd}," *IEEE Trans. Electron Devices*, vol. 66, no. 3, pp. 1482–1488, Mar. 2019, doi: 10.1109/TED.2019.2895700.

[12] X. Zhan, C. Shen, Z. Ji, J. Chen, H. Fang, F. Guo, and J. Zhang, "A dual-point technique for the entire I_D–V_G characterization into subthreshold region under random telegraph noise condition," *IEEE Electron Device Lett.*, vol. 40, no. 5, pp. 674–677, May 2019, doi: 10.1109/LED.2019.2903516.

[13] Y.-T. Chang, P.-W. Li, and H.-C. Lin, "Characterization of four-level random telegraph noise in a Gate-All-Around poly-Si nanowire transistor," in *Proc. Silicon Nanoelectronics Workshop (SNW)*, Jun. 2019, pp. 2007–2008, doi: 10.23919/SNW.2019.8782974.

[14] Z. Li, M. Sotto, F. Liu, M. K. Husain, H. Yoshimoto, Y. Sasago, D. Hisamoto, I. Tomita, Y. Tsuchiya, and S. Saito, "Random telegraph noise from resonant tunnelling at low temperatures," *Sci. Rep.*, vol. 8, no. 1, pp. 1–9, Dec. 2018, doi: 10.1038/s41598-017-18579-1.

[15] T. Gong, Q. Luo, X. Xu, J. Yu, D. Dong, H. Lv, P. Yuan, C. Chen, J. Yin, L. Tai, X. Zhu, Q. Liu, S. Long, and M. Liu, "Classification of three-level random telegraph noise and its application in accurate extraction of trap profiles in oxide-based resistive switching memory," *IEEE Electron Device Lett.*, vol. 39, no. 9, pp. 1302–1305, Sep. 2018, doi: 10.1109/LED.2018.2858245.

[16] T. Gong, Q. Luo, H. Lv, X. Xu, J. Yu, P. Yuan, D. Dong, C. Chen, J. Yin, L. Tai, X. Zhu, Q. Liu, S. Long, and M. Liu, "Unveiling the switching mechanism of a TaO_x/HfO_2 self-selective cell by probing the trap profiles with RTN measurements," *IEEE Electron Device Lett.*, vol. 39, no. 8, pp. 1152–1155, Aug. 2018, doi: 10.1109/LED.2018.2849730.

[17] R. Wang, S. Guo, Z. Zhang, J. Zou, D. Mao, and R. Huang, "Complex random telegraph noise (RTN): What do we understand?" in *Proc. IEEE Int. Symp. Phys. Failure Anal. Integr. Circuits (IPFA)*, Jul. 2018, pp. 1–7, doi: 10.1109/IPFA.2018.8452514.

[18] J. Zhang, Z. Zhang, R. Wang, Z. Sun, Z. Zhang, S. Guo, and R. Huang, "Comprehensive study on the 'Anomalous' complex RTN in advanced multi-fin bulk FinFET technology," in *IEDM Tech. Dig.*, no. 1, Dec. 2018, p. 17.

[19] H. Li, W. Wang, P. Huang, and Q. Li, "Fault diagnosis of rolling bearing using symmetrized dot pattern and density-based clustering," *Measurement*, vol. 152, Feb. 2020, Art. no. 107293, doi: 10.1016/j.measurement.2019.107293.

[20] M. F. Bukhori, T. Grasser, B. Kaczer, R. Hans, and A. Asenov, "'Atomistic' simulation of RTS amplitudes due to single and multiple charged defect states and their interactions," in *Proc. IEEE Int. Integr. Rel. Workshop Final Rep.*, Oct. 2010, pp. 76–79, doi: 10.1109/IIRW.2010.5706490.

[21] R. Wang, S. Guo, Z. Zhang, Q. Wang, D. Wu, J. Wang, and R. Huang, "Too Noisy at the Bottom?—Random telegraph noise (RTN) in advanced logic devices and circuits," in *IEDM Tech. Dig.*, Dec. 2018, p. 17.

[22] K. K. Hung, P. K. Ko, C. Hu, and Y. C. Cheng, "A unified model for the flicker noise in metal-oxide-semiconductor field-effect transistors," *IEEE Trans. Electron Devices*, vol. 37, no. 3, pp. 654–665, Mar. 1990, doi: 10.1109/16.47770.

[23] L. K. J. Vandamme and F. N. Hooge, "What do we certainly know about $1/f$ noise in MOSTs?" *IEEE Trans. Electron Devices*, vol. 55, no. 11, pp. 3070–3085, Nov. 2008, doi: 10.1109/TED.2008.2005167.

[24] F. M. Puglisi, A. Padovani, L. Larcher, and P. Pavan, "Random telegraph noise: Measurement, data analysis, and interpretation," in *Proc. IEEE 24th Int. Symp. Phys. Failure Anal. Integr. Circuits (IPFA)*, Jul. 2017, pp. 1–9, doi: 10.1109/IPFA.2017.8060057.

[25] C. Marquez, N. Rodriguez, F. Gamiz, R. Ruiz, and A. Ohata, "Electrical characterization of random telegraph noise in fully-depleted Silicon-On-Insulator MOSFETs under extended temperature range and back-bias operation," *Solid-State Electron.*, vol. 117, pp. 60–65, Mar. 2016, doi: 10.1016/j.sse.2015.11.022.
[26] P. Ren, R. Wang, X. Jiang, Y. Qiu, C. Liu, and R. Huang, "Experimental study on the oxide trap coupling effect in metal oxide semiconductor field effect transistors with HfO_2 gate dielectrics," *Appl. Phys. Lett.*, vol. 104, no. 26, Jun. 2014, Art. no. 263512, doi: 10.1063/1.4885394.

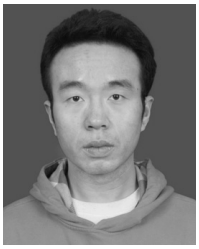

XUEPENG ZHAN received the bachelor's and Ph.D. degrees in micro-electronics and solid-state electronics from the College of Electronic Science and Engineering, Jilin University, in 2012 and 2017, respectively. As a postdoctor, he worked in Shandong University and Liverpool John Moores University. He is currently an Associate Research Fellow with the School of Information Science and Engineering (ISE), Shandong University. Meanwhile, he also does some joint work at the State Key Laboratory of High-End Server and Storage Technology, Jinan. His research interests focus on femtosecond laser processing and microelectronic device characterization.

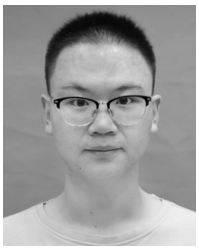

YIFANG XI received the B.S. degree in electronic information engineering from Shandong University, Shandong, China, in 2019, where he is currently pursuing the master's degree with the Institute of the Information Science and Engineering. His current research interests include in-memory computing and nano-device fabricating.

QIANWEN WANG received the bachelor's degree in physics from Qufu Normal University, in 2017. She is currently pursuing the Ph.D. degree with the School of Physics and the School of Information Science and Engineering, Shandong University. Her research interest focuses on the reliability of nano devices including cold source FET technology.

WEIQIANG ZHANG received the bachelor's degree in communication engineering from Central South University, in 2019. He is currently pursuing the master's degree in electronic science and technology with Shandong University. His research interest is the characterization and fabrication of ferroelectric HZO films.

ZHIGANG JI (Member, IEEE) received the B.Eng. degree in electrical engineering from Tsinghua University, in 2003, the M.Eng. degree in microelectronics from Peking University, in 2006, and the Ph.D. degree in microelectronics from Liverpool John Moores University, in 2010. He was the Reader with Liverpool John Moors University (LJMU). He is currently a Professor of nanoelectronics with Shanghai Jiao Tong University (STJU). He has authored or coauthored more than 100 journals and conference papers covering the research on the degradation phenomena of SiON, high-k, 2D materials, and multiple-gate devices and characterization of Ge/III-V, MIM devices, and emerging memories. His current research interests focus on characterization, modeling and design of reliable, low-power, and high-performance computation systems, and motivated by both evolutionary and revolutionary advances in nanoelectronics.

JIEZHI CHEN (Senior Member, IEEE) received the Ph.D. degree from the Department of Informatics and Electronics, The University of Tokyo, in 2009. He joined the R&D Center, Toshiba Corporation, in 2010. He is currently a Professor with the School of Information Science and Engineering, Shandong University, China. His research interests include the characterization and process engineering of nano-scale transistors and non-volatile memories, with main focus on reliability physics. He has published many articles in journals and conference proceedings and acted as a reviewer of several international journals. His work on nanoscale devices and device reliabilities has been the leading author or the corresponding author for more than ten times in VLSI Symposium and IEEE International Electron Device Meeting (IEEE IEDM), since 2008. He also serves as a Technical Program Committee (TPC) Member for IEDM, in 2016 and 2017, and a TPC Member of Silicon Nanoelectronics Workshop, since 2018, the IEEE International Reliability Physics Symposium, since 2019, and the IEEE International Memory Workshop, in 2020.